AIP | Journal of Applied Physics

Analytical device model for graphene bilayer field-effect transistors using weak nonlocality approximation

V. Ryzhii, M. Ryzhii, A. Satou, T. Otsuji, and V. Mitin

Citation: J. Appl. Phys. **109**, 064508 (2011); doi: 10.1063/1.3560921
View online: http://dx.doi.org/10.1063/1.3560921
View Table of Contents: http://jap.aip.org/resource/1/JAPIAU/v109/i6
Published by the American Institute of Physics.

Analytical device model for graphene bilayer field-effect transistors using weak nonlocality approximation

V. Ryzhii,[1,4,a)] M. Ryzhii,[1,4] A. Satou,[2,4] T. Otsuji,[2,4] and V. Mitin[3]
[1]*Computational Nanoelectronics Laboratory, University of Aizu, Aizu-Wakamatsu 965-8580, Japan*
[2]*Research Institute for Electrical Communication, Tohoku University, Sendai 980-8577, Japan*
[3]*Department of Electrical Engineering, University at Buffalo, State University of New York, New York 14260, USA*
[4]*Japan Science and Technology Agency, CREST, Tokyo 107-0075, Japan*

(Received 30 August 2010; accepted 1 February 2011; published online 21 March 2011)

We develop an analytical device model for graphene bilayer field-effect transistors (GBL-FETs) with the back and top gates. The model is based on the Boltzmann equation for the electron transport and the Poisson equation in the weak nonlocality approximation for the potential in the GBL-FET channel. The potential distributions in the GBL-FET channel are found analytically. The source-drain current in GBL-FETs and their transconductance are expressed in terms of the geometrical parameters and applied voltages by analytical formulas in the most important limiting cases. These formulas explicitly account for the short-gate effect and the effect of drain-induced barrier lowering. The parameters characterizing the strength of these effects are derived. It is shown that the GBL-FET transconductance exhibits a pronounced maximum as a function of the top-gate voltage swing. The interplay of the short-gate effect and the electron collisions results in a nonmonotonic dependence of the transconductance on the top-gate length. © *2011 American Institute of Physics*. [doi:10.1063/1.3560921]

I. INTRODUCTION

The unique properties of graphene layers, graphene nanoribbon arrays, and graphene bilayers[1–3] along with graphene nanomeshes[4] make them promising for different nanoelectronic device applications. The gapless energy spectrum of graphene layers allows us to use them in terahertz and mid-infrared detectors and lasers.[5–9] However, the gapless energy spectrum of graphene layers (GLs) is an obstacle for creating transistor digital circuits based on graphene field-effect transistors (G-FETs) due to relatively strong interband tunneling in the FET off-state.[10,11] The reinstatement of the energy gap in graphene-based structures like graphene nanoribbons, graphene nanomeshes, and graphene bilayers appears to be unavoidable to fabricate FETs with a sufficiently large on/off ratio. Recently, the device dc and ac characteristics of graphene nanoribbon and graphene bilayer FETs (which are referred to as GNR-FETs and GBL-FETs, respectively) were both numerically and analytically assessed.[12–19] The device characteristics of GNR-FETs operating in near ballistic and drift-diffusion regimes can be calculated analogously with those of nanowire- and carbon nanotube-FETs (see, for instance Refs. 20–22 and references therein). The GBL-FET characteristics can, in principle, be found using the same approaches as those realized previously for more customary FETs with a two-dimensional electron system in the channel.[23–31] However, some important features of GBL-FETs, in particular, the dependence of both the electron density and the energy gap in different sections of the GBL-FET channel on the gate and drain voltages should be considered,[32–34] along with the "short-gate" effect and the drain-induced barrier lowering.[29]

In this paper, we use a substantially generalized version of the GBL-FET analytical device model[17,18] to calculate the characteristics of GBL-FETs (the threshold voltages, current-voltage characteristics, and transconductance) in different regimes and analyze the possibility of a significant improvement of the ultimate performance of these FETs by a shortening of the gate and a decrease of the gate layer thickness. The device model under consideration which presents the GBL-FET characteristics in closed analytical form allows a simple and clear evaluation of the ultimate performance of GBL-FETs and their comparison. The following effects are considered: (a) dependences of the electron density and energy gap in different sections of the channel on the applied voltages and the inversion of the gated section charge; (b) degeneracy of the electron system, particularly in the source and drain sections of the channel; (c) the short-gate effect and the effect of drain-induced barrier lowering; (d) electron scattering in the channel.

Our model is based on the Boltzmann kinetic equation for the electron system in the GBL-FET and the Poisson equation in the weak nonlocality approximation.[35,36] The use of the latter allows us to find the potential distributions along the channel in the most interesting cases and analytically obtain the GBL-FET characteristics.

The paper is organized as follows. In Sec. II, the GBL-FET device model under consideration is presented and the features of GBL-FET operation are discussed. In Sec. III, the main equations of the model are cited. The general formulas for the source-drain current and the GBL-FET transconductance simplified for the limiting cases (far below the threshold, near threshold, and at low top-gate voltages corresponding to the on-state) are also presented. In this section, the source-drain current and the GBL-FET transconductance are expressed in terms of

a)Electronic mail: v-ryzhii@u-aizu.ac.jp.

the Fermi energy in the source and drain contacts and the height of the potential barrier in the channel. To find the barrier height, the Poisson equation is solved for different limiting cases in Sec. IV. The obtained potential distributions are used for the derivation of the explicit formulas for the source-drain current and the transconductance as functions of the applied voltages and geometrical parameters. Section V is a brief discussion of some effects (role of the device geometry, electron scattering, charge inversion in the channel, and interband tunneling), which influence the GBL-FET characteristics. In Sec. VI, we draw the main conclusions. Some reference data related to the voltage dependences of the Fermi energy and the energy gap in different sections of the GBL-FET channel are contained in the Appendix.

II. DEVICE MODEL AND FEATURES OF OPERATION

We consider a GBL-FET with the structure shown in Fig. 1. It is assumed that the back gate, which is positively biased by the pertinent voltage $V_b > 0$, provides the formation of the electron channel in the GBL between the ohmic source and drain contacts. A relatively short top gate serves to control the source-drain current by forming the potential barrier (its height Δ_m depends on the top gate voltage V_t and other voltages) for the electrons propagating between the contacts.

We shall assume that the GBL-FETs under the conditions when the electron systems in the source and drain sections are degenerate, i.e., $\varepsilon_F \gg k_B T$. This implies that the back gate voltage is sufficiently high to induce the necessary electron density in the source and drain sections.

In the GBL-FET the energy gap is electrically induced by the back gate voltage[32–34] (see also Ref. 18). Thus in GBL-FETs, the back gate plays a dual role: it provides the formation of the electron channel and the energy gap. Since the electric field component directed perpendicular to the GBL plane in the channel section below the top gate (gated section) is determined by both V_b and V_t, the energy gap can be different in different sections of the GBL channel: $E_{g,s}$ (source section), E_g (gated section), and $E_{g,d}$ (drain section).[17,18] At sufficiently strong top-gate voltage ($V_t < V_{th} < 0$, where V_{th} is the threshold voltage), the gated section becomes depleted. Since the energy gaps in GBLs are in reality not particularly wide, at a further moderate increase in $|V_t|$, the gated section of the channel becomes filled with holes (inversion of the charge in the gated section) if $V_t < V_{in} < V_{th}$, where V_{in} is the inversion voltage. As a result, the GBL-FETs with moderate energy gaps are characterized by the threshold and inversion voltages: $V_{th} < 0$ and $V_{in} < 0$. The explicit formulas for V_{th} and V_{in} shall be given in the following section. The cases $V_t = V_{th}$ and $V_t = V_{in}$ correspond to the alignment of the Fermi level in the source section of the channel with the conduction band bottom and the valence band top, respectively, in the gated section.

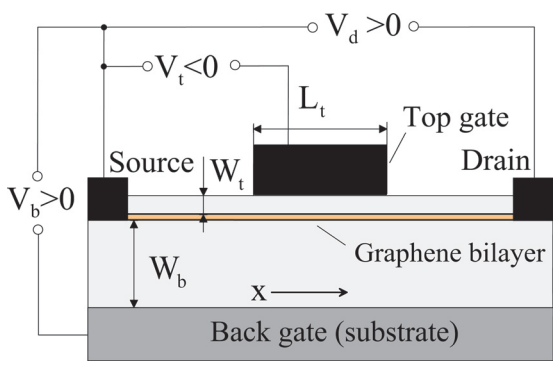

FIG. 1. (Color online) Schematic view of the GBL-FET structure.

III. MAIN EQUATIONS OF THE MODEL

Due to the relatively high energy of optical phonons in graphene, the electron scattering in the GBL-FET channel is primarily due to disorder and acoustic phonons. Considering such quasielastic scattering, the quasiclassical Boltzmann kinetic equation governing the steady state electron distribution function $f_{\mathbf{p}} = f_{\mathbf{p}}(x)$ in the gated section of the channel can be presented as

$$v_x \frac{\partial f_{\mathbf{p}}}{\partial x} + e\frac{\partial \varphi}{\partial x}\frac{\partial f_{\mathbf{p}}}{\partial p_x} = \int d^2\mathbf{q} w(q)(f_{\mathbf{p}+\mathbf{q}} - f_{\mathbf{p}})\delta(\varepsilon_{\mathbf{p}+\mathbf{q}} - \varepsilon_{\mathbf{p}}). \quad (1)$$

Here $e = |e|$ is the electron charge, $\varepsilon_{\mathbf{p}} = p^2/2m$, where m is the electron effective mass in GBL, $\mathbf{p} = (p_x, p_y)$ is the electron momentum in the GBL plane ($z = 0$), $w(q)$ is the probability of the electron scattering upon disorder and acoustic phonons with the variation of the electron momentum by the quantity $\mathbf{q} = (q_x, q_y)$, $v_x = p_x$ and axis x is directed in this plane (from the source contact to the drain contact, i.e., in the direction of the current). For simplicity, we disregard the effect of the "Mexican hat" (see, for instance, Ref. 34) and a deviation of the real energy spectrum in the GBL from the parabolic one (the latter can be marked in the source and drain sections with relatively high Fermi energies). The effective mass in GBLs $m = \gamma_1/2v_W$, where $\gamma_1 \simeq 0.35 - 0.43$ eV is the inter-layer hopping integral and $v_W \simeq 10^8$ cm/s is the characteristic velocity of electrons and holes in GLs,[3,34–36] so that $m \simeq (0.03 - 0.04)m_0$, where m_0 is the bare electron mass. One of the potential advantages of GBL-FETs is the possibility of ballistic transport even if the top-gate length L_t is not small. In such GBL-FETs, one can neglect the right-hand side term in Eq. (1).

As in Refs. 10, 15, 37, and 38 we use the following equation for the electric potential $\varphi = \varphi(x) = \psi(x,z)|_{z=0}$ in the GBL plane:

$$\frac{(W_b + W_t)}{3}\frac{\partial^2 \varphi}{\partial x^2} - \frac{\varphi - V_b}{W_b} - \frac{\varphi - V_t}{W_t} = \frac{4\pi e}{k}(\Sigma_- - \Sigma_+). \quad (2)$$

Here, Σ_- and Σ_+ are the electron and hole sheet densities in the channel, respectively, k is the dielectric constant of the layers between the GBL and the gates and W_b and W_t are the thicknesses of these layers. In the following, we use $W_b = W_t = W$ (except in Sec. V). Equation (2) is a consequence of the two-dimensional Poisson equation for the electric potential $\psi(x,z)$ in the GBL-FET gated section ($-L_t/2 \le x \le L_t/2$ and $-W_b \le z \le W_t$, where L_t is the length of the top gate) in the weak nonlocality approximation.[37] This equation provides the potential distributions, which can be obtained from the two-dimensional Poisson equation by expansion in powers of the parameter

$\delta = (W_b^3 + W_t^3)/15(W_b + W_t)/\mathcal{L}^2 = W^2/15\mathcal{L}^2$, where $\mathcal{L}$ is the characteristic scale of the lateral inhomogeneities (in the x-direction) assuming that $\delta \ll 1$, i.e., $\mathcal{L}$ is not too small. The lowest approximation in such an expansion leads to Shockley's gradual channel approximation, in which the first term on the left side of Eq. (2) is neglected.[39,40] The factor $1/3$ has appeared due to features of the Green function of the Laplace operator in the case of the geometry under consideration.

The boundary conditions for Eqs. (1) and (2) are presented as

$$f_{\mathbf{p}}\big|_{p_x \geq 0, x=-L_t/2} = f_{s,\mathbf{p}}, \quad f_{\mathbf{p}}\big|_{p_x \leq 0, x=L_t/2} = f_{d,\mathbf{p}}, \tag{3}$$

$$\varphi\big|_{x=-L_t/2} = 0, \quad \varphi\big|_{x=L_t/2} = V_d + (\varepsilon_{F,d} - \varepsilon_{F,s})/e = V_d^*, \tag{4}$$

where $f_{s,\mathbf{p}}$ and $f_{d,\mathbf{p}}$ are the electron distribution functions in the source and drain sections of the channel. The functions $f_{s,\mathbf{p}}$ and $f_{d,\mathbf{p}}$ are the Fermi distribution functions with the Fermi energies $\varepsilon_{F,s}$ and $\varepsilon_{F,d}$ which are determined by the back gate and drain voltages, V_b and V_d (Refs. 17 and 18) (also see the Appendix):

$$\varepsilon_{F,s} \simeq eV_b \frac{b}{(1+b)}, \quad \varepsilon_{F,d} \simeq e(V_b - V_d)\frac{b}{(1+b)}, \tag{5}$$

where $b = a_B/8W$, $a_B = k\hbar^2/me^2$ is the Bohr radius, and $\hbar$ is the reduced Planck constant. In the following, we shall assume that $b \ll 1$, so that $\varepsilon_{F,s} \simeq beV_b$ and $\varepsilon_{F,d} \simeq be(V_b - V_d)$. In particular, if $a_B = 4$ nm (GBL on SiO_2) and $W = 10$ nm, one obtains $b \simeq 0.05$. Due to a smallness of b, we shall disregard a distinction between V_d^* and V_d because $V_d - V_d^* \simeq bV_d \ll V_d$ (as shown in the Appendix). Restricting ourselves by the consideration of the GBL-FETs operation at not too high drain voltages, we also neglect the difference in the Fermi energies in the source and drain sections, i.e., put $\varepsilon_{F,d} \simeq \varepsilon_{F,s} = \varepsilon_F$.

The source-drain dc current density (current per unit length in the direction perpendicular to its flow) can be calculated using the following formulas:

$$J = \frac{4e}{(2\pi\hbar)^2}\int d^2\mathbf{p} v_x f_{\mathbf{p}} = \frac{e}{\pi^2\hbar^2}\int_{-\infty}^{\infty} dp_y \int_0^{\infty} dp_x v_x (f_{\mathbf{p}} - f_{-\mathbf{p}}). \tag{6}$$

In this case, Eq. (1) with boundary conditions (3) yields

$$f_{\mathbf{p}} - f_{-\mathbf{p}} \simeq \frac{\Theta(p_x^2/2m + e\varphi) - \Theta(p_x^2/2m + e\varphi - eV_d)}{1 + \exp[(p^2/2m + e\varphi - \varepsilon_F)/k_BT]}, \tag{7}$$

where T is the temperature, k_B is the Boltzmann constant, and $\Theta(\varepsilon)$ is the unity step function. Using Eqs. (6) and (7), we obtain

$$J = \frac{e}{\pi^2\hbar^2}\int_{-\infty}^{\infty} dp_y \int_{\Delta_m}^{\infty} d\xi \left\{ \frac{1}{1 + \exp[(p_y^2/2m + \xi - \varepsilon_F)/k_BT]} - \frac{1}{1 + \exp[(p_y^2/2m + \xi - \varepsilon_F + eV_d)/k_BT]} \right\}$$
$$= \frac{ek_BT}{\pi^2\hbar^2}\int_{-\infty}^{\infty} dp_y \left\{ \ln\left[\exp\left(\frac{\varepsilon_F - p_y^2/2m - \Delta_m}{k_BT}\right) + 1\right] - \ln\left[\exp\left(\frac{\varepsilon_F - p_y^2/2m - \Delta_m - eV_d}{k_BT}\right) + 1\right] \right\}. \tag{8}$$

Equation (8) can be presented in the following form:

$$J = J_0 \int_0^{\infty} dz \{\ln[\exp(\delta_m - z^2) + 1] - \ln[\exp(\delta_m - U_d - z^2) + 1]\}. \tag{9}$$

Here (see, for instance, Ref. 23)

$$J_0 = \frac{2\sqrt{2m}e(k_BT)^{3/2}}{\pi^2\hbar^2}, \tag{10}$$

is the characteristic current density, and $\delta_m = (\varepsilon_F - \Delta_m)/k_BT$ and $U_d = eV_d/k_BT$ are the normalized voltage swing and drain voltage, respectively. At $m = 4 \times 10^{-29}$ g and $T = 300$ K, $J_0 \simeq 2.443$ A/cm.

Figure 2 shows the dependences of the source-drain current J normalized by the value J_0 as a function of U_d calculated using Eq. (9) for different values of δ_m.

The GBL-FET transconductance g is defined as

$$g = \frac{\partial J}{\partial V_t}. \tag{11}$$

Equations (9) and (11) yield

$$g = J_0 \int_0^{\infty} dz \{[\exp(z^2 - \delta_m) + 1]^{-1} - [\exp(z^2 - \delta_m + U_d) + 1]^{-1}\}\left(-\frac{\partial \delta_m}{\partial V_t}\right). \tag{12}$$

The obtained formulas for the source-drain current and transconductance can be simplified in the following limiting cases.

A. High top-gate voltages

At high top-gate voltages, which correspond to the subthreshold voltage range, the barrier height exceeds the Fermi energy ($\Delta_m \gg \varepsilon_F$), so that $\delta_m \gg 1$. In this case (the electron system in the gated section is nondegenerate), using Eqs. (9) and (12) we obtain

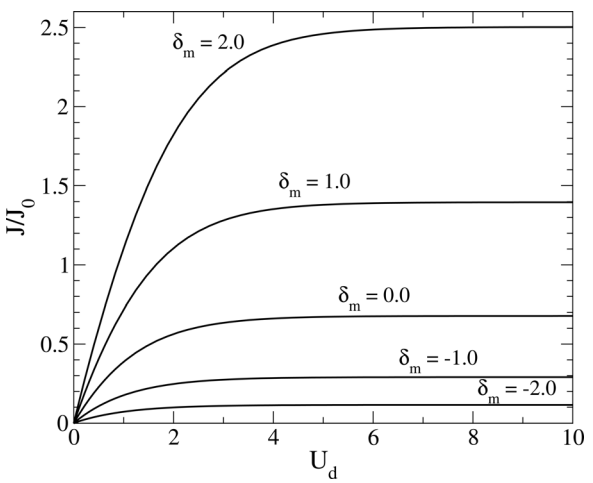

FIG. 2. Normalized source-drain current J/J_0 vs normalized drain voltage U_d at different values of the normalized top-gate voltage swing δ_m.

$$J = \frac{\sqrt{\pi}}{2} J_0 \exp\left(\frac{\varepsilon_F - \Delta_m}{k_B T}\right)\left[1 - \exp\left(-\frac{eV_d}{k_B T}\right)\right], \quad (13)$$

$$g = \frac{\sqrt{\pi}}{2}\frac{J_0}{k_B T}\exp\left(\frac{\varepsilon_F - \Delta_m}{k_B T}\right)\left[1 - \exp\left(-\frac{eV_d}{k_B T}\right)\right]\left(-\frac{\partial \Delta_m}{\partial V_t}\right). \quad (14)$$

B. Near threshold top-gate voltages

In this case, $\Delta_m \gtrsim \varepsilon_F$, i.e., $|\delta_m| \lesssim 1$, Eqs. (9) and (12) yield

$$J \simeq J_0 \frac{eV_d}{k_B T}\left[\zeta_1 + \zeta_2\left(\frac{\varepsilon_F - \Delta_m}{k_B T}\right)\right]\left[1 - \exp\left(-\frac{eV_d}{k_B T}\right)\right], \quad (15)$$

$$g \simeq \frac{J_0 eV_d}{(k_B T)^2}\zeta_2\left(-\frac{\partial \Delta_m}{\partial V_t}\right) \quad (16)$$

at low drain voltages $eV_d \lesssim k_B T$ ($U_d \lesssim 1$), and

$$J \simeq J_0\left[\zeta_0 + \zeta_1\left(\frac{\varepsilon_F - \Delta_m}{k_B T}\right)\right], \quad (17)$$

$$g \simeq \frac{J_0}{k_B T}\zeta_1\left(-\frac{\partial \Delta_m}{\partial V_t}\right) \quad (18)$$

at high drain voltages $eV_d \gg k_B T$ ($U_d \gg 1$). Here, $\zeta_0 = \int_0^\infty d\xi \ln[\exp(-\xi^2) + 1] \simeq 0.678$, $\zeta_1 = \int_0^\infty d\xi/[\exp(\xi^2) + 1] \simeq 0.536$, and $\zeta_2 = \int_0^\infty d\xi \exp(\xi^2)/[\exp(\xi^2) + 1]^2 \simeq 0.337$. In the limit $\varepsilon_F = \Delta_m$, Eqs. (13) and (14) provide the values J and g close to those obtained from Eqs. (17) and (18), which are rigorous in such a limit.

C. Low top-gate voltages

At low top-gate voltages, $\Delta_m < \varepsilon_F$, from Eqs. (9)

$$J \simeq \frac{2}{3} I_0[(\varepsilon_F - \Delta_m)^{3/2}\Theta(\varepsilon_F - \Delta_m) - (\varepsilon_F - \Delta_m - eV_d)^{3/2}\Theta(\varepsilon_F - \Delta_m - eV_d)], \quad (19)$$

$$g \simeq I_0[(\varepsilon_F - \Delta_m)^{1/2}\Theta(\varepsilon_F - \Delta_m) - (\varepsilon_F - \Delta_m - eV_d)^{1/2}\Theta(\varepsilon_F - \Delta_m - eV_d)]\left(-\frac{\partial \Delta_m}{\partial V_t}\right). \quad (20)$$

Here,

$$I_0 = \frac{2\sqrt{2me}}{\pi^2 \hbar^2}, \quad (21)$$

with $J_0 = I_0 (k_B T)^{3/2}$.

Using Eqs. (19) and (20), one obtains

$$J \simeq I_0 eV_d \sqrt{(\varepsilon_F - \Delta_m)} \simeq I_0 eV_d \sqrt{\varepsilon_F}\left(1 - \frac{\Delta_m}{2\varepsilon_F}\right), \quad (22)$$

$$g \simeq \frac{1}{2} I_0 \frac{eV_d}{\sqrt{\varepsilon_F}}\left(-\frac{\partial \Delta_m}{\partial V_t}\right) \quad (23)$$

at $eV_d \ll \varepsilon_F - \Delta_m$, and

$$J = \frac{2}{3} I_0 (\varepsilon_F - \Delta_m)^{3/2} \simeq \frac{2}{3} I_0 \varepsilon_F^{3/2}\left(1 - \frac{3\Delta_m}{2\varepsilon_F}\right), \quad (24)$$

$$g \simeq I_0 \sqrt{(\varepsilon_F - \Delta_m)}\left(-\frac{\partial \Delta_m}{\partial V_t}\right) \quad (25)$$

at $eV_d \gg \varepsilon_F - \Delta_m$.

The dependences shown in Fig. 2 implicitly describe the dependences of J calculated using the universal Eq. (9) on the back-gate, top-gate, and drain voltages and on the geometrical parameters. Equations (13)–(25) provide these dependences in most interesting limits. However, to obtain the explicit formulas for J as well as for g, one needs to determine the dependences of the barrier height Δ_m on all voltages and geometrical parameters. Since the electron densities in the gated section in the limiting cases under consideration are different, the screening abilities of the electron system in this section and the potential distributions are also different. The latter leads to different Δ_m versus V_t relations.

IV. POTENTIAL DISTRIBUTIONS, SOURCE-DRAIN CURRENT, AND TRANSCONDUCTANCE

To obtain the explicit dependences of the source-drain current and the transconductance on the gate voltages V_b and V_t and on the drain voltage V_d, one needs to find the relationship between the barrier height Δ_m and these voltages. This necessitates the calculations of the potential distribution in the channel. The latter can be found from Eq. (2) in an analytical form in the following limiting cases.

A. High top-gate voltages - sub-threshold voltage range ($\Delta_m \gg \varepsilon_F$)

When the barrier height Δ_m exceeds the Fermi energy ε_F, the electron density is low in the gated section and hence, one can disregard the contribution of the electron charge in this section. In such a limit, we arrive at the following equation for the potential:

$$\frac{d^2\varphi}{dx^2} - \frac{\varphi}{\Lambda_0^2} = \frac{F_0}{\Lambda_0^2}, \quad (26)$$

where $\Lambda_0 = \sqrt{2/3}W$ and $F_0 = -(V_b + V_t)/2$. Solving Eq. (26) considering boundary conditions (4), for the case of high top-gate voltages we obtain

$$\varphi = F_0\left[\frac{\cosh(x/\Lambda_0)}{\cosh(L_t/2\Lambda_0)} - 1\right] + V_d \frac{\sinh[(2x + L_t)/2\Lambda_0]}{\sinh(L_t/\Lambda_0)}. \quad (27)$$

Limiting our consideration by the GBL-FETs with not too short top gate ($L_t \gg W$), Eq. (27) can be presented as

$$\varphi \simeq -F_0\left[1 - 2\exp\left(-\frac{L_t}{2\Lambda_0}\right)\cosh\left(\frac{x}{\Lambda}\right)\right] + V_d \exp\left(-\frac{L_t}{2\Lambda_0}\right)\exp\left(\frac{x}{\Lambda_0}\right). \quad (28)$$

Equation (28) yields

$$\Delta_m \simeq eF_0\left(1-\frac{1}{\eta_0}\right)-\frac{eV_d}{2\eta_0} = -\frac{e(V_b+V_t)}{2}\left(1-\frac{1}{\eta_0}\right)-\frac{eV_d}{2\eta_0}, \quad (29)$$

where $\eta_0 = \exp(L_t/2\Lambda_0)/2$. Simultaneously, for the position of the barrier top one obtains

$$x_m = -\frac{\Lambda_0}{2}\ln\left(1+\frac{V_d}{F_0}\right) = -\frac{\Lambda_0}{2}\ln\left(1-\frac{2V_d}{V_b+V_t}\right). \quad (30)$$

The terms on the right-hand side of Eq. (29) containing the parameter η_0 reflect the effect of the top-gate geometry (finiteness of its length). This effect is weakened with the increasing top barrier length L_t. The effect of drain-induced barrier lowering in the case under consideration is described by the last term on the right-hand side of Eq. (29).

Equation (29) yields $(\partial\Delta_m/\partial V_t) = -(e/2)(1-\eta_0^{-1})$. Invoking Eqs. (13) and (14), we obtain

$$J = \frac{\sqrt{\pi}}{2}J_0\exp\left[\frac{e(V_t-V_{th})}{2k_BT}\left(1-\frac{1}{\eta_0}\right)\right] \times\left[1-\exp\left(-\frac{eV_d}{k_BT}\right)\right]\exp\left(\frac{eV_d}{2\eta_0 k_BT}\right), \quad (31)$$

$$g \simeq \frac{\sqrt{\pi}}{4}\frac{eJ_0}{k_BT}\exp\left[\frac{e(V_t-V_{th})}{2k_BT}\left(1-\frac{1}{\eta_0}\right)\right] \times\left[1-\exp\left(-\frac{eV_d}{k_BT}\right)\right]\exp\left(\frac{eV_d}{2\eta_0 k_BT}\right). \quad (32)$$

Here, $V_{th} = -[1+2b/(1-\eta_0^{-1})]V_b \simeq -(1+2b)V_b$. The rightmost factors on the right-hand sides of Eqs. (31) and (32), associated with the effect of drain-induced barrier lowering, lead to an increase in g with increasing V_d not only at $eV_d \sim k_BT$ but at $eV_d \gg k_BT$: $g \propto \exp(eV_d/2\eta_0 k_BT)$. One can see that in the range of the top-gate voltages under consideration, the GBL-FET transconductance exponentially decreases with increasing $|V_t+V_b|$ and

$$g \simeq \frac{Je}{2k_BT} \ll g_0 = \frac{\sqrt{\pi}}{4}\frac{eJ_0}{k_BT}, \quad (33)$$

where at $T = 300$ K the characteristic value of the transconductance is $g_0 \simeq 4330$ mS/mm.

B. Near threshold top-gate voltages ($\Delta_m \gtrsim \varepsilon_F$)

At $eV_d \lesssim k_BT \ll \varepsilon_F$, taking into account that the electron distribution is characterized by the equilibrium Fermi distribution function, the electron density in the gated section can be presented in the following form:

$$\sum \simeq \frac{2m}{\pi\hbar^2}(\varepsilon_F + e\varphi). \quad (34)$$

Considering this, we reduce Eq. (2) to

$$\frac{d^2\varphi}{dx^2}-\frac{\varphi}{\Lambda^2} = \frac{F}{\Lambda^2}. \quad (35)$$

Here,

$$\Lambda = \sqrt{\frac{a_BW}{12(1+2b)}} \simeq \sqrt{\frac{a_BW}{12}} = W\sqrt{\frac{2}{3}b},$$
$$F = \frac{[\varepsilon_F/e - b(V_b+V_t)]}{(1+2b)} \simeq -b(bV_b+V_t) \simeq -bV_t,$$

so that $\Lambda/\Lambda_0 \simeq \sqrt{b} < 1$. The solution of Eq. (35) with boundary condition (4) is given by

$$\varphi = F\left[\frac{\cosh(x/\Lambda)}{\cosh(L_t/2\Lambda)}-1\right]+V_d\frac{\sinh[(2x+L_t)/2\Lambda]}{\sinh(L_t/\Lambda)} \simeq -F\left[1-2\exp\left(-\frac{L_t}{2\Lambda}\right)\cosh\left(\frac{x}{\Lambda}\right)\right] + V_d\exp\left(-\frac{L_t}{2\Lambda}\right)\exp\left(\frac{x}{\Lambda}\right). \quad (36)$$

From Eq. (36) we obtain

$$\Delta_m \simeq eF\left(1-\frac{1}{\eta}\right)-\frac{eV_d}{2\eta} \simeq [\varepsilon_F - eb(V_b+V_t)]\left(1-\frac{1}{\eta}\right)-\frac{eV_d}{2\eta} \simeq -ebV_t\left(1-\frac{1}{\eta}\right)-\frac{eV_d}{2\eta}, \quad (37)$$

where $\eta = \exp(L_t/2\Lambda)/2$, and the position of the barrier top is

$$x_m \simeq -\frac{\Lambda}{2}\frac{V_d}{F} \simeq -\frac{\Lambda}{2b}\frac{V_d}{V_b}. \quad (38)$$

Since $\Lambda < \Lambda_0$, one obtains $\eta \gg \eta_0$, and the terms in Eq. (37) containing the parameter η can be disregarded. This implies that the effects of the top-gate geometry and drain-induced barrier lowering are much weaker (negligible) in the case of the top-gate voltages in question in comparison with the case of high top-gate voltages.

Substituting Δ_m from Eq. (37) into Eq. (16), for low drain voltages we arrive at

$$g \simeq \frac{J_0e^2V_d\zeta_2}{(k_BT)^2}\left(1-\frac{1}{\eta}\right)b. \quad (39)$$

At relatively high drain voltages ($eV_d > \varepsilon_F \gg k_BT$), the electron charge in the source portion of the gated section ($x \le x_m$, where x_m is the coordinate of the barrier top) is primarily determined by the electrons injected from the source. The electron injection from the drain at high drain voltages is insignificant. Hence, the electron charge in the drain portion of the gated section can be disregarded. In this case, Eq. (2) can be presented as

$$\frac{d^2\varphi}{dx^2}-\frac{\varphi}{\Lambda^2} = \frac{F}{\Lambda^2} \quad (40)$$

at $-L_t/2 \le x \le x_0$, and

$$\frac{d^2\varphi}{dx^2}-\frac{\varphi}{\Lambda_0^2} = \frac{F_0}{\Lambda_0^2} \quad (41)$$

at $x_0 \le x \le L_t/2$.

At the point $x = x_0$ corresponding to the condition $e\varphi|_{x=x_0} + \varepsilon_F = 0$, the solutions of Eqs. (40) and (41) should be matched:

$$\varphi|_{x=x_0-0} = \varphi|_{x=x_0+0} = -\frac{\varepsilon_F}{e}, \quad \left.\frac{d\varphi}{dx}\right|_{x=x_0-0} = \left.\frac{d\varphi}{dx}\right|_{x=x_0+0}. \quad (42)$$

Solving Eqs. (40) and (41) with conditions (4) and (42), we obtain the following formulas for the potential φ at $-L_t/2 \le x \le x_0$ and $x_0 \le x \le L_t/2$ as well as an equation for x_0:

$$\varphi = F\left[\frac{\cosh(x/\Lambda)}{\cosh(L_t/2\Lambda)} - 1\right] - \left[\frac{\varepsilon_F}{e} + F\frac{\cosh(x_0/\Lambda)}{\cosh(L_t/2\Lambda)} - F\right] \times \frac{\sinh[(x+L_t/2)/\Lambda)]}{\sinh[(x_0+L_t/2)/\Lambda)]}, \quad (43)$$

$$\varphi = F_0\left[\frac{\cosh(x/\Lambda_0)}{\cosh(L_t/2\Lambda_0)} - 1\right] + V_d\frac{\sinh[(x+L_t/2)/\Lambda_0]}{\sinh(L_t/\Lambda_0)} - \left[\frac{\varepsilon_F}{e} + F_0\frac{\cosh(x_0/\Lambda_0)}{\cosh(L_t/2\Lambda_0)} - F_0 + V_d\frac{\sinh[(x_0+L_t/2)/\Lambda_0]}{\sinh(L_t/\Lambda_0)}\right]\frac{\sinh[(x-L_t/2)/\Lambda_0]}{\sinh[(x_0-L_t/2)/\Lambda_0]}, \quad (44)$$

$$\frac{1}{\Lambda}\left\{F\frac{\sinh(x_0/\Lambda)}{\cosh(L_t/2\Lambda)} - \left[\frac{\varepsilon_F}{e} + F\frac{\cosh(x_0/\Lambda)}{\cosh(L_t/2\Lambda)} - F\right] \times \frac{\cosh[(x_0+L_t/2)/\Lambda)]}{\sinh[(x_0+L_t/2)/\Lambda)]}\right\} = \frac{1}{\Lambda_0}\left\{F_0\frac{\sinh(x_0/\Lambda_0)}{\cosh(L_t/2\Lambda_0)} + V_d\frac{\cosh[(x_0+L_t/2)/\Lambda_0]}{\sinh(L_t/\Lambda_0)} - \left[\frac{\varepsilon_F}{e} + F_0\frac{\cosh(x_0/\Lambda_0)}{\cosh(L_t/2\Lambda_0)} - F_0 + V_d\frac{\sinh[(x_0+L_t/2)/\Lambda_0]}{\sinh(L_t/\Lambda_0)}\right]\frac{\cosh[(x_0-L_t/2)/\Lambda_0]}{\sinh[(x_0-L_t/2)/\Lambda_0]}\right\}. \quad (45)$$

In the cases $V_b + V_t \simeq 0$ and $-(V_b + V_t) \gtrsim V_b \gg \varepsilon_F/e$, Eq. (45) yields $x_0 = -L_t/2 + \Lambda\ln[4bV_t/(\sqrt{b}+2b)(V_b+V_t)]$ and $x_0 \simeq -L_t/2 + 2\Lambda_0\varepsilon_F/[-e(V_b+V_t)] \simeq -L_t/2 + 2b\Lambda_0 V_b/[-(V_b+V_t)]$, respectively. When $-(V_b+V_t) \to +0$, the matching point shifts toward the channel center. If $-(V_b+V_t)$ increases, the matching point tends to the source edge of the channel. In this case, the role of the electron charge in the vicinity of the source edge diminishes, and the potential distribution tends to that given by Eq. (27).

At the threshold, the matching point x_0 coincides with the position of the barrier maximum x_m. Considering that at $x_0 = x_m$, both the left-hand and right-hand sides of Eq. (45) are equal to zero, for the barrier top height near the threshold at relatively high drain voltages we obtain the following:

$$\Delta_m \simeq eF_0\left(1 - \frac{1}{\eta_0}\right) - \frac{eV_d}{\eta_0} = -\frac{e(V_b+V_t)}{2}\left(1 - \frac{1}{\eta_0}\right) - \frac{eV_d}{\eta_0}, \quad (46)$$

$$x_m \simeq -\frac{L_t}{2} + \Lambda\ln\left(\frac{2F}{F-F_0}\right) \simeq -\frac{L_t}{2} + \Lambda\ln\frac{1}{b}. \quad (47)$$

Both Eqs. (29) and (46) correspond to the situations when the electron density in a significant portion of the channel is fairly low. However there is a distinction in the dependence of Δ_m on V_d (the pertinent coefficients differ by a factor of 2). This is because in the first case the barrier top is located near the channel center, whereas in the second case it is shifted to the vicinity of the source edge [compare Eqs. (30) and (47)].

Using Eqs. (19) and (50), we obtain $(\partial\Delta_m/\partial V_t) = -(e/2)(1-\eta_0^{-1})$ and arrive at the following formula for the transconductance near the threshold, i.e., when $V_t \simeq V_{th}$

$$J \simeq J_0\left[\zeta_0 + \zeta_1\frac{e(V_t - V_{th})}{2k_BT}\left(1 - \frac{1}{\eta_0}\right)\right], \quad (48)$$

$$g \simeq \frac{J_0 e}{k_BT}\frac{\zeta_1}{2}\left(1 - \frac{1}{\eta_0}\right) = g_{th}. \quad (49)$$

Here, as above, $V_{th} \simeq -(1+2b)V_b$. In particular, Eqs. (48) and (49) at $V_t = V_{th}$, yield $J_{th} \simeq J_0\zeta_0$. For a GBL-FET with $L_t = 40$ nm, $W = 10$ nm, at $T = 300$ K one obtains $J_{th} \simeq 1.656$ A/cm and $g_{th} \simeq 2167$ mS/mm.

C. Low top-gate voltages ($\Delta_m < \varepsilon_F$)

At relatively low top-gate voltages when $\Delta_m < \varepsilon_F$, the electron system is degenerate not only in the source and drain sections but in the gate section as well. In this top-gate voltage range, the spatial variation of the potential is characterized by $\Lambda \simeq W\sqrt{2b/3}$. As a result, for Δ_m one obtains an equation similar to Eq. (37). Since $\Lambda < \Lambda_0 \ll L_t$, the parameter determining the effect of the top-gate geometry and the effect of drain-induced barrier lowering is $\eta = \exp(L_t/2\Lambda)/2 \gg \eta_0$. As a consequence, one can neglect the effects in question in the top-gate voltage range under consideration. As a result, one can arrive at

$$J \simeq \frac{2}{3}I_0 e^{3/2}[b(V_t - V_{th})]^{3/2} - [b(V_t - V_{th} - V_d]^{3/2} \quad (50)$$

when $V_d \le b(V_t - V_{th})$,

$$J \simeq \frac{2}{3}I_0 e^{3/2}[b(V_t - V_{th})]^{3/2}, \quad (51)$$

when $V_d > b(V_t - V_{th})$, and

$$\frac{\partial\Delta_m}{\partial V_t} = -be. \quad (52)$$

Considering Eq. (51), at low top-gate voltages we obtain

$$g \simeq \frac{beI_0}{2}\frac{eV_d}{\sqrt{\varepsilon_F}} \simeq \frac{\sqrt{b}e^{3/2}I_0}{2}\frac{V_d}{\sqrt{V_b}} \quad (53)$$

when $eV_d \gg \varepsilon_F - \Delta_m \simeq be(V_b + V_t)$, and

$$g \lesssim beI_0\sqrt{\varepsilon_F} \simeq b^{3/2}e^{3/2}I_0\sqrt{V_b} = g_{on} \quad (54)$$

when $eV_d \ll \varepsilon_F - \Delta_m \simeq be(V_b + V_t)$. As follows from Eqs. (33) and (34), the transconductance is proportional to a small

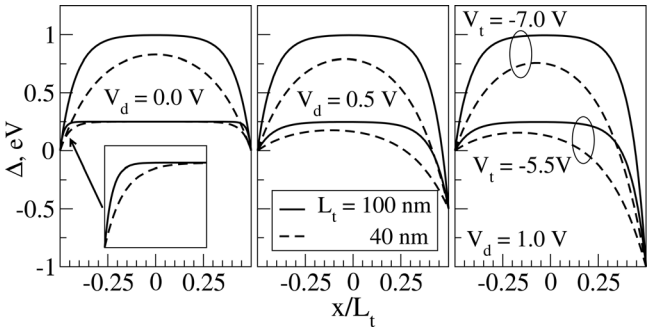

FIG. 3. Barrier profile $\Delta = -e\phi$ at different top-gate voltage V_t and drain voltage V_d for GBL-FETs with different top-gate length L_t. Upper and lower pairs of curves correspond to $V_t - V_{th} = -1.5$ V and $V_t - V_{th} \simeq 0$, respectively; $W = 10$nm, $b = 0.05$, and $V_b = 5.0$ V.

parameter $b^{3/2}$. This is because the effect of the top-gate potential is weakened due to a strong screening by the degenerate electron system in the gated section. As a result, the transconductance at low top-gate voltages is smaller than that at the top-gate voltage corresponding to the threshold. Assuming that $b = 0.05$ and $V_b = 5$ ($\varepsilon_F \simeq 0.25$ eV), we obtain $g_{on} \simeq 1467$ mS/mm. Comparing Eqs. (49) and (54), we find $g_{on}/g_{th} \propto b^{3/2}\sqrt{eV_b/k_BT} \simeq 0.158$ and $g/g_{th} \lesssim g_{on}/g_{th} \simeq 0.68$.

Since the source-drain current at high top-gate voltages decreases exponentially when $-V_t$ increases, the transconductance decreases as well.

Figure 3 shows the barrier (conduction band) profile $\Delta = -e\varphi$ in the GBL-FETs calculated using Eqs. (27), (36), and (44) for different applied voltages and top-gate lengths. As demonstrated, the barrier height naturally decreases with increasing $V_t - V_{th}$. At the threshold ($V_t = V_{th}$), the barrier height is equal to the Fermi energy (at $b = 0.05$ and $V_b = 5$ V, $\varepsilon_F \simeq 0.25$ eV). One can see that the shortening of the top-gate leads to a marked decrease in the barrier height (the short-gate effect). The source-drain current as a function of the drain voltage for different top-gate voltage swings is demonstrated in Fig. 4. The dependences corresponding to $V_t - V_{th} < 0$, $V_t - V_{th} = 0$, and $V_t - V_{th} > 0$ were calculated using formulas from subsections A, B, and C, respectively.

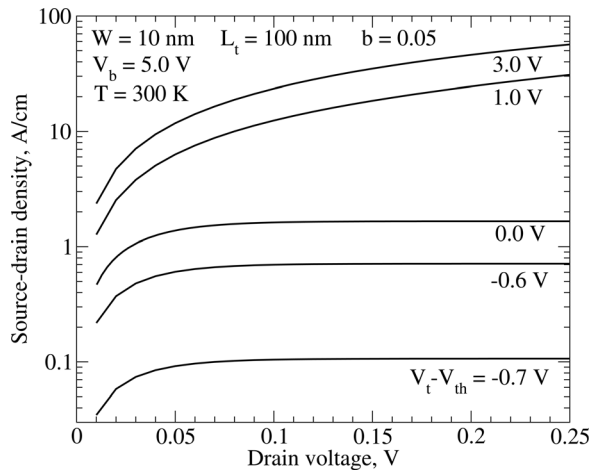

FIG. 4. Source-drain current J vs drain voltage V_d at different values of the top-gate voltage swing $V_t - V_{th}$.

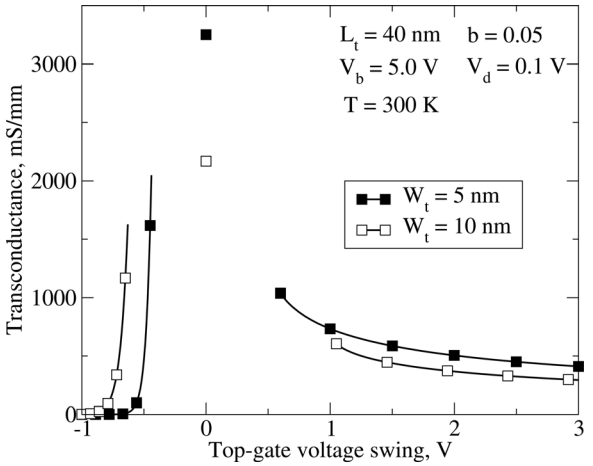

FIG. 5. Transconductance g vs top-gate voltage swing $V_t - V_{th}$.

Figure 5 shows that the transconductance as a function of the top-gate voltage swing exhibits a pronounced maximum at $V_t \simeq V_{th}$. This maximum is attributed to the following. At high top-gate voltages, the effect of screening is insignificant due to low electron density in the channel. As a result, the height of the barrier top is rather sensitive to the top-gate voltage variations. The source-drain current in this case is exponentially small so that the transconductance is small. In contrast, at low top-gate voltages, the screening by the electrons in the channel is effective, leading to a much weaker control of the barrier height by the top voltage [pay attention to parameter $b \ll 1$ in Eqs. (50)–(54)]. Despite this fact, a strong source-drain current provides a moderate value of the transconductance. However, in the near threshold voltage range, both the sensitivity of the barrier height and the source-drain current to the top-gate voltage are fairly large.

V. DISCUSSION

A. Role of geometrical parameters

In the main part of the paper, we assumed that the thicknesses of the gate layers are equal to each other: $W_b = W_t = W$. If $W_b \neq W_t$, the formulas obtained above should be slightly modified. In particular, near the threshold $(\partial\Delta_m/\partial V_t) = -(e/(1 + W_t/W_b)(1 - \eta_0^{-1})$, so that the transconductance instead of Eq. (49) is given by

$$g \simeq \frac{J_0 e}{k_B T}\frac{\zeta_1}{(1 + W_t/W_b)\zeta_0}\left(1 - \frac{1}{\eta_0}\right) \simeq \frac{J_0 e}{k_B T}\frac{\zeta_1}{(1 + W_t/W_b)\zeta_0}. \quad (55)$$

As follows from the comparison of Eqs. (49) and (55), changing W_t, in particular, from $W_t = W_b$ to $W_t = W_b/2$, leads to an increase in the transconductance at the top-gate voltages near the threshold of 50% (compare the g versus $V_t - V_{th}$ dependences in Fig. 5 for $W_b = W_t = 10$ nm and $W_b = 10$ nm and $W_t = 5$ nm).

As demonstrated above, shortening of the top gate can result in the deterioration of the GBL-FET characteristics.

This effect is characterized by parameters η and η_0, which strongly depend on the top-gate length L_t. This effect gives rise to a decrease in the transconductance if L_t becomes smaller. However, in the range of large L_t the electron collisions can play a substantial role. This leads to the transconductance roll-off with increasing L_t. The effect of drain-induced barrier lowering is also characterized by parameters η and η_0. As follows from Sec. IV, at sub-threshold, the effect of drain-induced barrier lowering results in the appearance of the factor $\exp(eV_d/2\eta_0 k_B T)$ [see Eqs. (31) and (32)]. This factor can provide a marked increase in J and g with increasing drain voltage in GBL-FETs with relatively short top gates. For example, at $W = 40$ nm, $L_t = 40$ nm, $T = 300$ K, and $V_d = 0.25$ V, this factor is about 2.37.

The obtained characteristics comprise parameter b, which is proportional to the Bohr radius a_B. An increase in a_B when a large-k substrate, say, HfO_2 ($a_B = 20$ nm) is used instead of the SiO_2 substrate ($a_B = 4$ nm), and, consequently, an increase in b leads to higher sensitivity of the barrier height to the applied voltages and, hence, to higher transconductance.

B. Effect of electron scattering

As shown above, the potential distributions in the main part of the gated section are fairly flat. This implies that to determine the effect of electron scattering associated with disorder and acoustic phonons one can use Eq. (2) with the collisional term following the approach applied in Ref. 17. The interaction of electrons with optical phonons, particularly with optical phonons in the substrate, can be effective in the gate-drain section at elevated drain voltages. However, even relatively strong scattering on optical phonons in this section should not markedly affect the dc characteristics under consideration, although it can be essential for the ac characteristics. Considering the case here when the elastic scattering mechanisms under consideration are strong so that they lead to an effective isotropization of the electron distribution, one can find that the values of the source-drain current and the transconductance obtained in the previous section for the ballistic transport should be multiplied by a collision factor C. This factor is equal to $C_\infty = \sqrt{2\pi k_B T/m}/L_t \nu$, where $\nu = mw/2$ is the collision frequency we use $w(q) = w = \text{const}$. It characterizes the fraction of the electrons injected into the gated section and those reflected back due to the collisions. To obtain the GBL-FET characteristics with the top-gate lengths in a wide range (to follow the transition from the ballistic electron transport to the collision-dominated transport), we use for the collision factor the following interpolation formula:

$$C = \frac{1}{1 + L_t/L_{\text{scat}}}, \tag{56}$$

where $L_{\text{scat}} = \sqrt{2\pi k_B T/m}/\nu$ is the characteristic scattering length. Figures 6 and 7 show the dependences of the transconductance maximum (approximately at $V_t = V_{th}$) on the top-gate length calculated for GBL-FETs with different W_t. The scattering length is assumed to be ∞ (ballistic transport), 500 nm, and 75 nm. At $T = 300$ K, this corresponds to

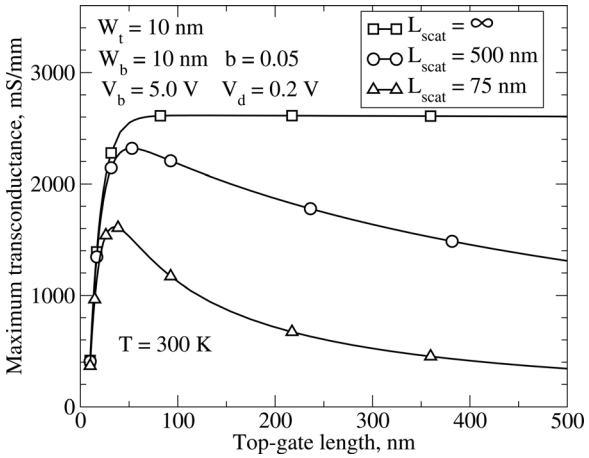

FIG. 6. Maximum transconductance g vs top-gate length L_t for $W_t = 10$ nm.

the collision frequencies $\nu = 0$, $\nu \simeq 1.14 \times 10^{12}$ s^{-1} (the electron mobilities $\mu \simeq 1.75 \times 10^5$ cm^2/V s) and $\nu \simeq 7.6 \times 10^{12}$ s^{-1} ($\mu \simeq 2.63 \times 10^4$ cm^2/V s), respectively). One can see that in the case of essential electron collisions, g versus L_t dependences exhibit pronounced maxima. This is attributed to an interplay of two effects: the short-gate effect (weakening of the barrier controllability by the top-gate voltage when L_t decreases) and the effect of collisions, which is reinforced when L_t becomes larger (which decreases the current). As follows from Figs. 6 and 7, the electron collisions can lead to a dramatic decrease in the transconductance.

C. Charge inversion in the gated section

At sufficiently high top-gate voltages $V_t < V_{in}$ when $\Delta_m > \varepsilon_F + E_g$, the top of the valence band in the gated section of the channel can be markedly populated by holes (inversion of the gated section charge), so that the term in the right-hand side of Eq. (2) becomes negative. The latter inequality corresponds to the following value of the inversion voltage [see Eqs. (A4) and (A5)]:

$$V_{in} = -V_b\left(1 + 2b + \frac{d_0}{W}\right) \simeq V_{th}\left(1 + \frac{d_0}{W}\right). \tag{57}$$

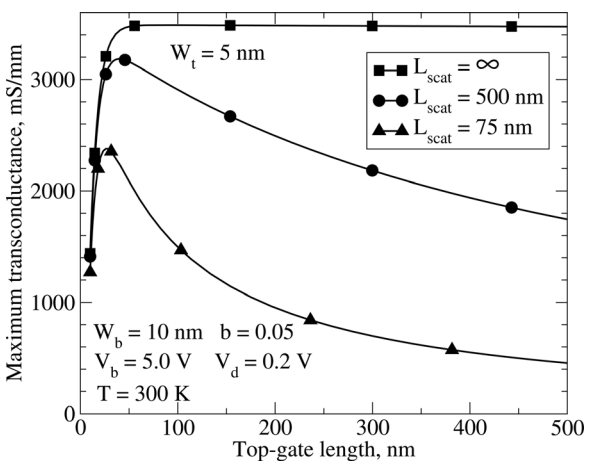

FIG. 7. The same as in Fig. 6 but for $W_t = 5$ nm.

The hole charge provides an effective screening of the transverse electric field in the gated section. This leads to weakening of the sensitivity of the barrier height and the source-drain current on the top gate voltage V_t (Ref. 15) and, hence, to a decrease in the transconductance. This pattern is valid at the dc voltages or when the characteristic time of their variation is long in comparison with the characteristic times of the thermogeneration of holes and the tunneling between the channel side regions and the gated section.[15,17] In the situation when the hole recharging of the gated section of the channel is a relatively slow process, the ac transconductance at the frequencies higher than the characteristic recharging frequency can substantially exceed the dc transconductance.

D. Interband tunneling

At elevated top-gate voltages ($V_t < V_{in}$), the interband tunneling of electrons from the conduction band in the source to the valence band in the gated section as well as from the valence band in the gated section to the conduction band in the drain can be essential. At high drain voltages the latter tunneling processes can be particularly pronounced. This can result in an elevated source-drain current despite a rather high barrier. To limit the tunneling, the back-gate voltage, which mainly determines the energy gap, should be high enough. A decrease in the gate layer thicknesses also promotes the tunneling suppression. For example, if $W = (5-10)$ nm, $V_b = -V_t = 5$ V, the energy gap in the gated section of the channel $E_g \simeq 0.17 - 0.34$ eV [see Eq. (A4)]. Despite some attempts to calculate the tunneling currents in G-FETs and GBL-FETs (see, for instance, Refs. 11 and 19), the problem for GBL-FETs remains open. This is because the spatial nonuniformity of the energy gap in the channel and its nonlinear spatial dependence (particularly near the drain edge) associated with the features of the potential distribution under the applied voltages. Generalizing Eq. (A4), we obtain $E_g = ed[V_b - \varphi(x)]/2W$, hence the energy gap varies from $E_g = E_{g,s} \simeq edV_b/W$ at $x = -L_t/2$ to $E_g = E_{g,s} \simeq ed(V_b - V_d/2W$ at $x = L_t/2$. It reaches a maximum $E_g = d(eV_b + \Delta_m)/2W$ at $x = x_m$. One can see that $E_{g,d}$ can be markedly smaller than E_g, especially at drain voltages that are not too small. Due to this, the deliberation of the tunneling in GBL-FETs requires a sufficiently rigorous device model (which could include the formulas for the potential distribution obtained above) and numerical approach.

VI. CONCLUSIONS

We demonstrated that the developed device model allows us to derive the GBL-FET characteristics: the potential distributions along the channel, the dependences of the source-drain current and the transconductance on the applied voltages, and the geometrical parameters as closed-form analytical expressions. The key element of the model, which provides an opportunity to solve the problem analytically, is the use of the Poisson equation in the weak nonlocality approximation. In particular, the model accounts for the effect of screening of the transverse electric field by the electron charge in the channel, the short-gate effect, and the effect of drain-induced barrier lowering. The parameters η_0 and η characterizing the strength of these effects in the cases of an essentially depleted channel and strong screening were expressed via the geometrical parameters and the Bohr radius. As shown, the GBL-FET transconductance exhibits a pronounced maximum as a function of the top-gate voltage swing. The interplay of the short-gate effect and the electron collisions results in a nonmonotonic dependence of the transconductance on the top-gate length. The obtained analytical formulas for the potential barrier height, the source-drain current, and the transconductance can be used for GBL-FET optimization by the proper choice of the thicknesses of gate layers, the top-gate length, and the bias voltages.

ACKNOWLEDGMENTS

The authors are grateful to H. Watanabe for stimulating comments and to V. V. V'yurkov for providing Ref. 31. The work was supported by the Japan Science and Technology Agency, CREST, Japan.

APPENDIX: VOLTAGE DEPENDENCES OF THE FERMI ENERGY AND THE ENERGY GAP

Disregarding the effect of "Mexican-hat" and the nonparabolicity of the electron energy spectrum, the density of states can be considered independent of the energy (in the energy range under consideration). Taking this into account, the electron Fermi energies and the energy gaps in the source and drain sections of the GBL-FET channel are, respectively, given by Refs. 17 and 18 ($W_b = W_t = W$),

$$\varepsilon_{F,s} = \frac{k_B T}{(1+b)} \ln\left[\exp\left(\frac{beV_b}{k_B T}\right) - 1\right], \tag{A1}$$

$$\varepsilon_{F,d} = \frac{k_B T}{(1+b)} \ln\left[\exp\left(\frac{be(V_b - V_d)}{k_B T}\right) - 1\right], \tag{A2}$$

$$E_{g,s} = \frac{edV_b}{2W}, \quad E_{g,s} = \frac{ed(V_b - V_d)}{2W}. \tag{A3}$$

Here $a_B = k\hbar^2/me^2$, $b = a_B/8W$, and $d \lesssim d_0$, where $d_0 \simeq 0.34$ nm (Ref. 32) is the spacing between the graphene layers in the GBL, while d stands for the effective spacing accounting for the screening of the transverse electric field by GBL (polarization effect). In the portion of the gated section essentially occupied by electrons and its depleted portion, one obtains

$$E_g = \frac{ed(V_b - V_t)}{2W}, \quad E_g = \frac{ed_0(V_b - V_t)}{2W}, \tag{A4}$$

respectively. Due to $a_B \gg d$, from Eqs. (A1)–(A4) one obtains $\varepsilon_{F,s} \geq \varepsilon_{F,d} > E_{g,s} \geq E_{g,d}$. At $V_t < 0$, E_g can significantly exceed $E_{g,s}$ and $E_{g,d}$. In the case of strong degeneracy of the electron system, Eqs. (A1) and (A2) yield

$$\varepsilon_{F,s} \simeq eV_b \frac{a_B/8W}{(1+b)}, \quad \varepsilon_{F,d} \simeq e(V_b - V_d)\frac{b}{(1+b)}. \tag{A5}$$

The quantity $\varepsilon_{F,d}$ is given by the same equations in which, however, V_b is substituted by $V_b - V_d$. As a result,

$$\varepsilon_{F,s} - \varepsilon_{F,d} \simeq \frac{beV_d}{1+b} \simeq beV_d, \tag{A6}$$

$$eV_d^* = eV_d + \varepsilon_{F,d} - \varepsilon_{F,s} \simeq \frac{eV_d}{1+b}. \quad \text{(A7)}$$

Since parameter b in reality is small, so that $\varepsilon_{F,s} - \varepsilon_{F,d} \simeq be V_d \ll eV_d$ and $V_d^* \simeq V_d$ we put $\varepsilon_{F,s} = \varepsilon_{F,d} = \varepsilon_F$ and substitute V_d^* by V_d.

[1]C. Berger, Z. Song, T. Li, X. Li, A. Y. Ogbazhi, R. Feng, Z. Dai, A. N. Marchenkov, E. H. Conrad, P. N. First, and W. A. de Heer, J. Phys. Chem. B. **108**, 19912 (2004).
[2]K. S. Novoselov, A. K. Geim, S. V. Morozov, D. Jiang, M. I. Katsnelson, I. V. Grigorieva, S. V. Dubonos, and A. A. Firsov, Nature (London) **438**, 197 (2005).
[3]A. H. Castro Neto, F. Guinea, N. M. R. Peres, K. S. Novoselov, and A. K. Geim, Rev. Mod. Phys. **81**, (2009).
[4]J. Bai, X. Zhong, S. Jiang, Y. Huang, and X. Duan, Nat.Nanotechnol. **5**, 190 (2010).
[5]V. Ryzhii, M. Ryzhii, and T. Otsuji, J. Appl. Phys. **101**, 083114 (2007).
[6]F. Rana, IEEE Trans. Nanotechnol. **7**, 91 (2008).
[7]F. Xia, T. Murleer, Y.-M. Lin, A. Valdes-Garsia, and P. Avouris, Nat. Nanotechnol. **4**, 839 (2009).
[8]V. Ryzhii, M. Ryzhii, V. Mitin, and T. Otsuji, J. Appl. Phys. **107**, 054512 (2010).
[9]V. Ryzhii, A. A. Dubinov, T. Otsuji, V. Mitin, and M. S. Shur, J. Appl. Phys. **107**, 054505 (2010).
[10]V. Ryzhii, M. Ryzhii, and T. Otsuji, Appl. Phys. Express **1**, 013001 (2008).
[11]V. Ryzhii, M. Ryzhii, and T. Otsuji, Phys. Status Solidi A, **205** 1527 (2008).
[12]Y. Quyang, Y. Yoon, J. K. Fodor, and J. Guo, Appl. Phys. Lett. **89** 203107 (2006).
[13]G. Fiore and G. Iannaccone, IEEE Electron Device Lett. **28**, 760 (2007).
[14]G. Liang, N. Neophytou, D. E. Nikonov, and M. S. Lundstrom, IEEE Trans. Electron Devices **54**, 677 (2007).
[15]V. Ryzhii, M. Ryzhii, A. Satou, and T. Otsuji, J. Appl. Phys. **103**, 094510 (2008).
[16]M. Ryzhii, A. Satou, V. Ryzhii, and T. Otsuji, J. Appl. Phys. **104**, 114505 (2008).
[17]V. Ryzhii, M. Ryzhii, A. Satou, T. Otsuji, and N. Kirova, J. Appl. Phys. **105**, 104510 (2009).
[18]M. Ryzhii and V. Ryzhii, Phys. Rev. B **79**, 245311 (2009).
[19]M. Cheli, G. Fiori, and G. Iannaccone, IEEE Trans. Electron Devices **56**, 2979 (2009).
[20]S. O. Koswatta, S. Hasan, M. S. Lundstrom, M. P. Anantram, and D. E. Nikonov, Appl. Phys. Lett. **89**, 023125 (2006).
[21]M. Lenzi, P. Palestri, E. Gnani, S. Reggiani, A. Gnudi, D. Esseni, L. Selmi, and G. Baccarani, IEEE Trans. Electron Devices **55**, 2087 (2008).
[22]S. Fregonese, J. Gouet, C. Manex, and T. Zimmer, IEEE Trans. Electron Devices **56**, 1184 (2009).
[23]K. Natori, J. Appl. Phys. **76**, 4881 (1994).
[24]A. Rahman, J. Guo, S. Datta, and M. S. Lundstrom, IEEE Trans. Electron Devices **50**, 1853 (2003).
[25]F. G. Pikus and K. K. Likharev, Appl. Phys. Lett. **71**, 3661 (1997).
[26]V. A. Sverdlov, T. J Walls, and K. K. Likharev, IEEE Trans. Electron Devices **50**, 1926 (2003).
[27]N. Sano, Phys. Rev. Lett. **93**, 246803 (2004).
[28]G. Mugnaini and G. Iannaccone, IEEE Trans. Electron Devices **52**, 1802 (2005).
[29]R. Kim, P. A. Neophytou, G. Klimeck, and M. S. Lundstrom, J. Vac. Sci. Technol. B **26**, 1628 (2008).
[30]R. Akis, N. Faralli, D. K. Ferry, S. M. Goodnick, K. A. Phatak, and M. Saratini, IEEE Trans. Electron Devices **56**, 2935 (2009).
[31]A. N. Khomyakov and V. V. V'yurkov, Russian Microelectron. **38**, 393 (2009).
[32]T. Ohta, A. Q. Bostwick, T. Seyller, K. Horn, and E. Rotenberg, Science **333**, 951 (2006).
[33]E. McCann, Phys. Rev. B **74**, 161403 (2006).
[34]E. V. Castro, K. S. Novoselov, S. V. Morozov, N. M. R. Peres, J. M. B. Lopes dos Santos, L. Nilsson, F. Guinea, A. K. Geim, and A. H. Castro Neto, J. Phys.: Condens. Matter **22**, 175503 (2010).
[35]E. A. Henriksen, Z. Jiang, L.-C. Tung, M. E. Schwartz, M. Takita, Y. J. Wang, P. Kim, and H. Stormer, Phys. Rev. Lett. **100**, 087403 (2008).
[36]M. Orlita and M. Potemski, Semicond. Sci. Technol. **25**, 063001 (2010).
[37]A. A. Sukhanov and Y. Y. Tkach, Sov. Phys. Semicond. **18**, 797 (1984).
[38]A. O. Govorov, V. M. Kowalev, and A. V. Chaplik, JETP Lett. **70**, 488 (1999).
[39]S. M. Sze, *Physics of Semiconductor Devices* (Wiley, New York, 1981).
[40]M. Shur, *Physics of Semiconductor Devices* (Prentice-Hall, New Jersey, 1990).